RECENT RESULTS IN e^+e^- ANNIHILATION FROM SLAC[*]

DANIEL L. SCHARRE

Stanford Linear Accelerator Center

Stanford University, Stanford, California 94305

Abstract

Recent results from the Mark II and Crystal Ball experiments at SLAC are presented. Mark II results include measurement of direct photon production at the ψ and observation of charmed baryon production. The Crystal Ball experiment sees evidence for a new state at 2.98 GeV produced in a radiative transition from the ψ'.

(Invited talk presented at the X International Symposium on Multiparticle Dynamics, Goa, India, September 25-29, 1979.)

I. Introduction

The general characteristics of particle production at intermediate energies (defined here to be center-of-mass energies between the ψ and T masses) in e^+e^- annihilation have come out of the work done over the last few years at SLAC and DESY. More recent work has aimed at achieving an understanding of some of the details of particle production, particularly in relation to QCD and charmonium predictions. In this talk, I present some recent results from both the Mark II and Crystal Ball collaborations. Both experiments have been taking data at the SLAC e^+e^- storage ring facility SPEAR. From the Mark II, results on the inclusive γ and π^0 momentum distributions at the ψ are presented. Evidence for direct γ production is observed. The results are not in complete agreement with leading-order QCD predictions. The Mark II collaboration also sees direct evidence for a charmed baryon signal at a mass of 2.285 GeV and has measured the absolute branching ratio of this state into $pK^-\pi^+$. Finally, the inclusive γ momentum distribution at the ψ' (from the Crystal Ball) is presented. They see evidence for a radiative transition to a state at 2.98 GeV which might be interpreted as the η_c. This state fits more easily into the charmonium level scheme than the previously observed state at 2.83 GeV.

II. Mark II Magnetic Detector

The members of the Mark II collaboration are given in Ref. 1. The detector itself has been described in detail elsewhere[2] and only a brief description of the particle detection will be presented in this talk. A schematic of the Mark II magnetic detector is shown in Fig. 1. Charged tracks are reconstructed from hits in the sixteen cylindrical drift chamber layers which provide solid angle coverage over 85% of 4π sr. The resulting

Vacuum Chamber

Pipe Counter (2 layers, scintillation counters)

Drift Chamber (16 layers)

Time of Flight Counters (48 total)

Solenoid Coil

Liquid Argon Shower Counter (8 barrel modules)

Iron Flux Return

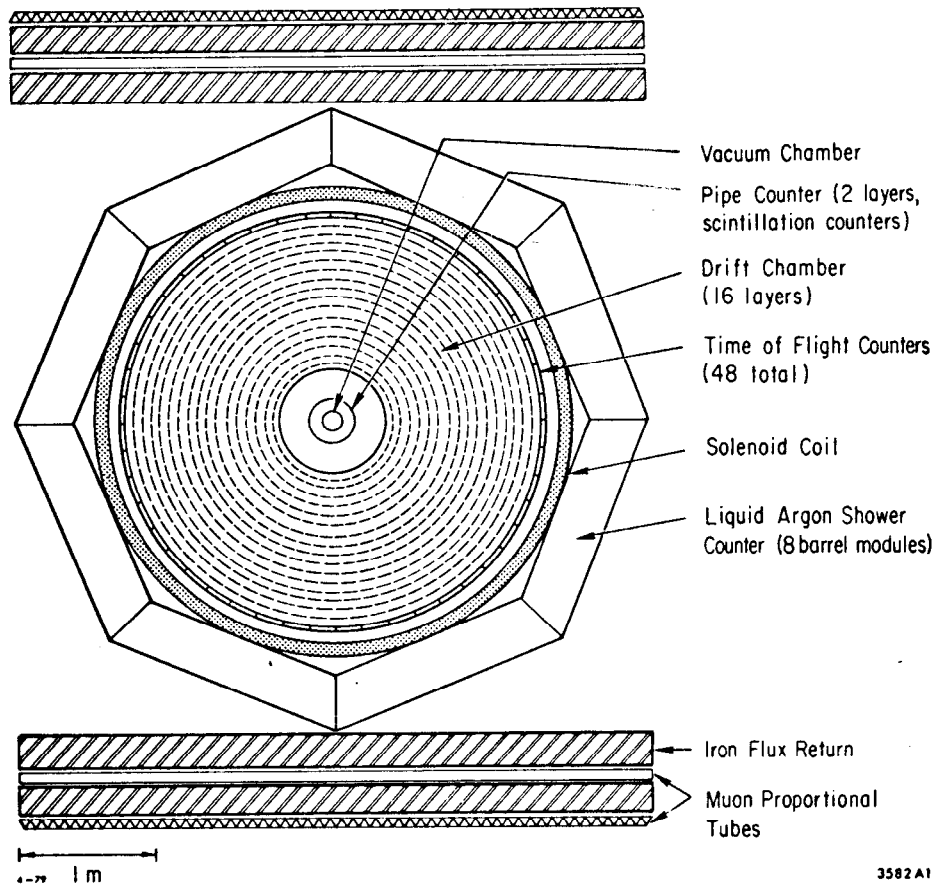Muon Proportional Tubes

1 m

3582A1

Fig. 1. Schematic of the Mark II magnetic detector looking along the beam direction. Not shown are the muon proportional counters on both sides of the detector and the end-cap shower counters.

charged track momentum resolution is

$$\delta p/p = \left[(0.0145)^2 + (0.005p)^2 \right]^{\frac{1}{2}} ,$$

where p is the momentum in GeV. The trigger requires two or more charged tracks, each with transverse momentum greater than 100 MeV, to be within the solid angle covered by the drift chamber, one of which must be within the central region of the drift chamber which covers 67% of 4π sr.

Outside the drift chamber are 48 scintillation counters which provide charged particle time-of-flight information over 75% of 4π sr. The average flight path is 1.85 m which leads to an average resolution of $\sigma = 0.30$ ns for hadrons.

Photons are detected primarily in the eight lead-liquid argon (LA) shower counter modules which surround the solenoid, covering approximately 64% of 4π sr. The rms energy resolution for detected photons is given approximately by $\delta E/E = 0.12 E^{-\frac{1}{2}}$ (E in GeV).

In addition, there are proportional tubes for muon detection outside the detector (partially shown in Fig. 1) and shower counters (not shown in the figure) which cover the endcap regions.

III. Direct Photon Production at the ψ

First-order QCD calculations predict that a significant fraction of the hadronic decays of heavy quark-antiquark $^3S_1$ resonances (such as the ψ) result in the production of direct γ's (i.e., γ's not coming from secondary decays of π^0's or η's).[3] The hadronic decay of the ψ must proceed via an intermediate state consisting of at least 3 color-octet gluons. The lowest-order QCD diagram corresponds to the 3-gluon decay shown in Fig. 2(a). By replacing one of the outgoing gluon lines with a photon, as in Fig. 2(b), one obtains a diagram which results in the production of direct γ's. From lowest-order perturbation theory, the leading-order calculation for the ratio of the partial widths to these two final state gives

$$B_\gamma = \Gamma(\psi \to \gamma gg)/\Gamma(\psi \to ggg) = (\alpha/\alpha_s)\, C(e_Q/e)^2 \quad ,$$
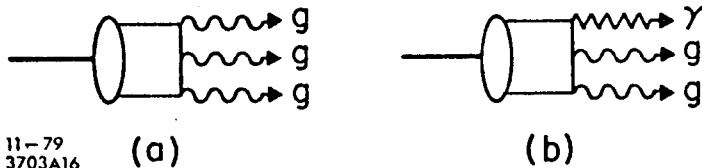
11-79
3703A16 **(a)**   **(b)**

Fig. 2. (a) Leading-order diagram for hadronic production from the ψ.
(b) Diagram leading to the production of direct γ's.

where C = 36/5 is a color SU(3) factor, e_Q is the charge of the charmed quark, and α_s is the color fine-structure constant. For $\alpha_s = 0.18$,[4] one calculates $B_\gamma = 13\%$ for the integral

over all x. Equating the direct decay of the ψ into hadrons with the 3-gluon decay, and correcting for second-order electromagnetic decays, the lowest-order QCD prediction for the branching ratio for direct γ decays from the ψ is 8%.

The momentum spectrum for γ's produced in such decays is predicted to be roughly proportional to x, where x is the fraction of the beam energy taken by the γ, and peak near x = 1 (see Fig. 3). In the event of resonance production (e.g., gluonium final states) in the recoil system, one might expect a deviation from the lowest-order distribution as shown by the dashed curve in Fig. 3. However, it must be remembered that this calculation includes only the leading-order diagrams. It is expected that the observed distribution will be softer than the leading-order prediction since radiative effects and the masses of the final-state hadrons are not considered, but no calculation has been made. A similar calculation for the decay width of a heavy quark-antiquark bound state indicates that higher-order effects are of the same magnitude as lower-order terms,[5] thus making it difficult to provide accurate theoretical predictions.
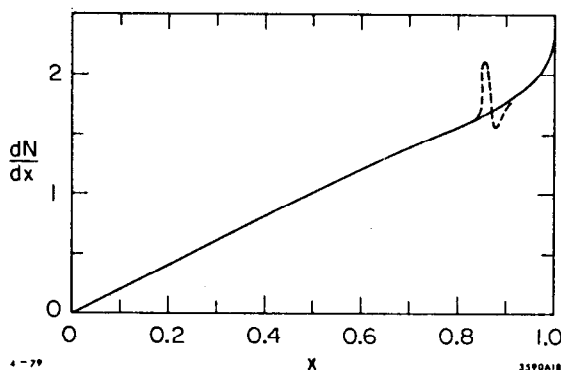

Fig. 3. Inclusive direct γ momentum distribution as a function of x calculated to lowest order in QCD. Dashed curve shows the effect of resonance production in the final state.

The measurement of the inclusive γ and π° momentum distributions has been made using three different methods of analysis as a check on possible systematic errors. The first method of analysis makes use of a sample of 92,000 produced ψ events from the decay $\psi' \rightarrow \psi\pi^{+}\pi^{-}$ which is obtained by requiring that the missing mass from observed pairs of oppositely

charged pions be consistent with the mass of the ψ (m_ψ). The background from accidental combinations falling in the ψ mass region is estimated using events in bands on either side of the peak and subtracted. This sample of ψ events is identified purely from the π^+ and π^- and has no trigger bias arising from the ψ decay.

Although no corrections to the data are required for trigger efficiency, corrections must be made for the geometric acceptance and detection efficiency of the γ's and π^o's. γ's are detected in the eight LA shower counter modules surrounding the solenoid. The detection efficiency (including geometric acceptance) is obtained using Monte Carlo simulation of the electromagnetic shower development[6] in the Mark II detector assuming isotropic production of γ's. These calculated efficiencies agree with efficiencies obtained by measuring the relative fraction of events with one and two observed γ's from the decays $\psi \rightarrow \pi^+\pi^-\pi^o$ and $\psi \rightarrow \pi^+\pi^-\pi^+\pi^-\pi^o$. The efficiency as a function of γ energy is shown in Fig. 4.
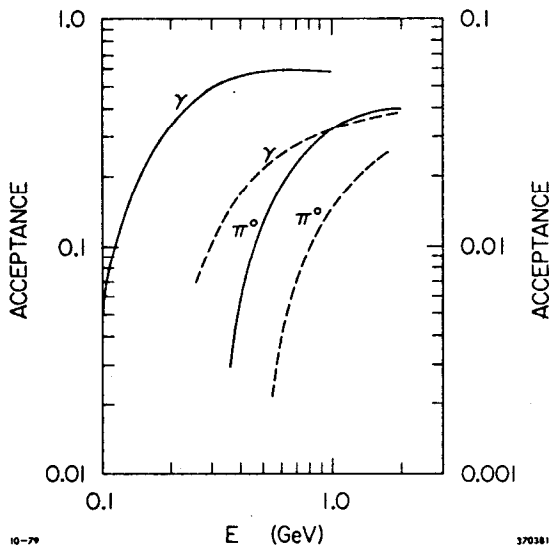

Fig. 4. Solid curves show the detection efficiency (including geometry) for γ's and π^o's detected in the LA as functions of energy (left ordinate). Dashed curves show the detection efficiency for γ's which convert prior to entering the drift chamber and π^o's with one converted γ (right ordinate).

Neutral pions are reconstructed by combining pairs of γ's, each of which is required to have momentum greater than 150 MeV. Pairs with invariant mass between 0.075 and 0.200 GeV are considered to be π^o candidates. The π^o signal is extracted after subtraction of a background whose shape is a function of momentum. The background shape is obtained by combining real photons and

"pseudo-photons" from the same event. Pseudo-photons are created in the analysis program by pretending that charged particles are π^o's and allowing them to decay into pseudo-photons. In this method of background subtraction, it is assumed that the charged particle and π^o momentum distributions are similar. Resolution and efficiency effects are included in the generation of pseudo-photons in order to simulate the observed photon spectrum. The background distribution is normalized to the data in the mass region between 0.3 and 1.0 GeV. Finally, a correction is made for the tails of the π^o which fall outside the specified mass cuts. The π^o detection efficiency is calculated by Monte Carlo and includes the effects of all cuts used in the π^o reconstruction and data analysis. The efficiency as a function of energy is shown in Fig. 4.

The second method of analysis makes use of a sample of 280,000 observed $\geq$ 2 prong hadron events taken near the peak of the ψ(3095) resonance. In order to measure the inclusive γ and π^o momentum distributions without trigger bias, only γ's which convert in the 0.06-radiation length of material preceeding the drift chamber layers (i.e., the vacuum pipe, the scintillation counters surrounding the vacuum pipe, and the lexan inner surface of the drift chamber) are used in the analysis. The photons are reconstructed from measurement of the momenta of the resulting e^+ and e^- in the drift chamber. Neutral pions are reconstructed from combinations of a converted γ and a γ observed in the LA. The π^o background is subtracted as described above. As essentially all γ's and π^o's which are measured satisfy the trigger requirement, there is no trigger bias in this method of analysis. In addition to freedom from trigger bias, this method of analysis provides excellent energy resolution for detected γ's. The resolution is given approximately by $\delta E/E = 0.022 \; E^{\frac{1}{4}}$ (E in GeV). Unfortunately, the statistics are poor because the photon conversion

probability is small. The γ and π^o detection efficiencies (shown in Fig. 4) are calculated by Monte Carlo.

The third method of analysis uses the same sample of ψ events as method 2. However, only γ's detected in the LA rather than converted γ's are used in the analysis. This method has the largest statistics. γ and π^o reconstruction is identical to that used in method 1. However, there is now the added complication of determining the trigger efficiency. This efficiency is measured using the sample of events from the decay $\psi' \rightarrow \psi\pi^+\pi^-$. As a function of γ or π^o momentum p, the trigger efficiency is calculated as the fraction of events which satisfy the trigger requirement after elimination of the recoiling π^+ and π^- from the event. The resulting trigger efficiency as a function of $x = 2p/m_\psi$ for events with γ's or π^o's detected in the LA is shown in Fig. 5. (A similar determination of the trigger efficiency has been made using the converted γ events and gives consistent results.) In a similar manner, the number of produced ψ events corresponding to the 280,000 observed hadron events is calculated to be 435,000 from the overall trigger efficiency obtained from the sample of ψ events originating from ψ' decays.
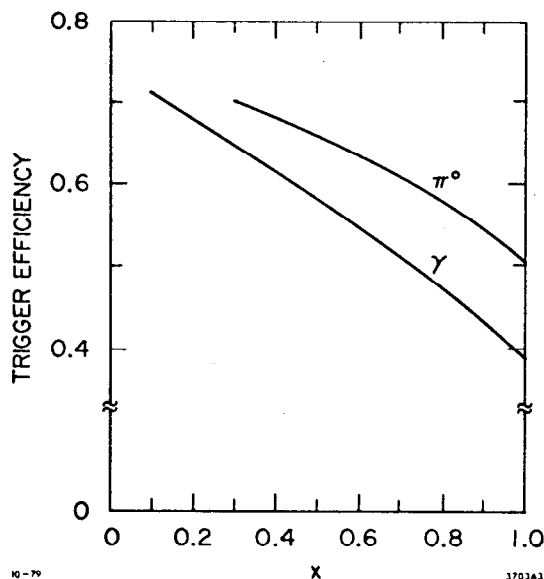
Figure 6 shows the inclusive γ momentum distributions $(1/N_{tot})dN/dx$ as determined by each of the three methods of analysis as functions of $x = 2p/m_\psi$. N_{tot} is the total number of produced ψ's. (For method 1, the γ momenta are Lorentz-transformed into the rest frame of the ψ.) The error bars represent the statistical errors only. Overall systematic errors are approximately ±20% and

Fig. 5. Trigger efficiency as a function of x for events with γ's or π^o's detected in the LA, where $x = 2p/m_\psi$.
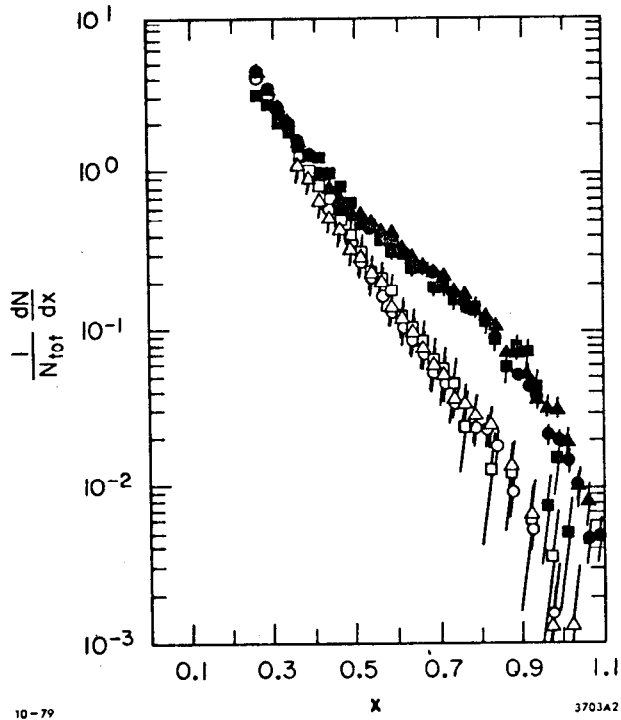
-8-

Fig. 6. Inclusive γ momentum distributions $(1/N_{tot})dN/dx$ as functions of x for the three methods of analysis. The solid data points represent the measured γ spectra and the error bars are statistical only. The open points represent the predicted γ spectra from the measured π^0 and η distributions. The error bars on these points include both statistical and relative systematic errors as discussed in the text. The data obtained from the sample of ψ events from ψ' decays (method 1) are displayed as triangles. The converted photon data (method 2) are displayed as squares. The LA data (method 3) are displayed as circles.

may vary slowly with x. Corrections for γ detection efficiency (and for method 3, trigger efficiency) have been made. Background due to the e^+e^- final state in which one of the electrons radiates a γ is eliminated by removing events with 2 charged prongs (not including the $\pi^+\pi^-$ system from the ψ' decay in method 1 and the converted γ in method 2), one of which is identified as an electron with momentum greater than 1.0 GeV and with cosθ < -0.8, where θ is the angle between the electron and the observed γ. Background due to the reaction $e^+e^- \to \gamma\gamma$ (in the sample of events with converted γ's) is removed by eliminating events with no charged particles besides the

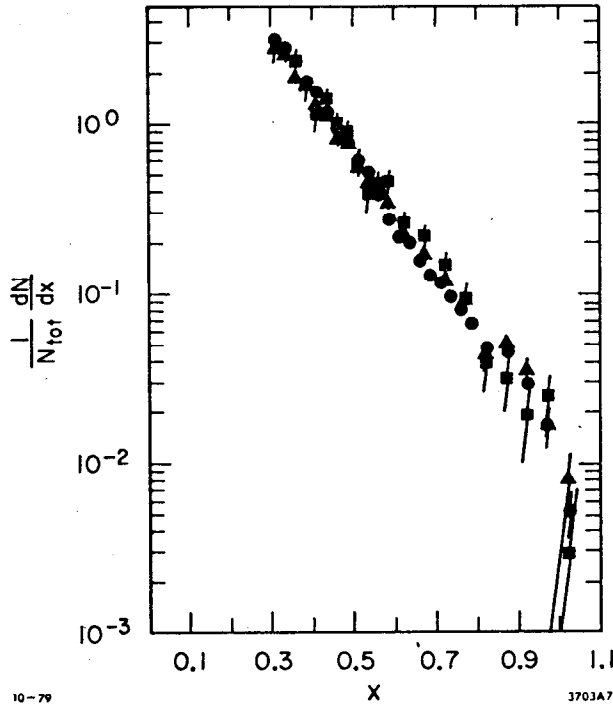electron-positron pair from the conversion which have a high energy γ detected in the LA opposite the converted γ. The three methods give consistent results for the inclusive distribution. The spread of the data from the three methods provides an indication of how well the systematic errors are understood.

Fig. 7. Inclusive π^0 momentum distributions $(1/N_{tot})dN/dx$ as functions of $x = 2p/m_\psi$. The error bars represent the statistical errors only. The symbol convention is identical to that used in Fig. 6.

Figure 7 shows the inclusive π^0 momentum distributions $(1/N_{tot})dN/dx$. Corrections for π^0 detection efficiency and trigger efficiency have been made. Systematic errors of $\pm 30\%$ are not shown in the figure. Again there is consistency between the results of the three methods. Using preliminary results for the charged pion inclusive distribution from the data, a comparison between the charged and neutral pion cross sections has been made. The $\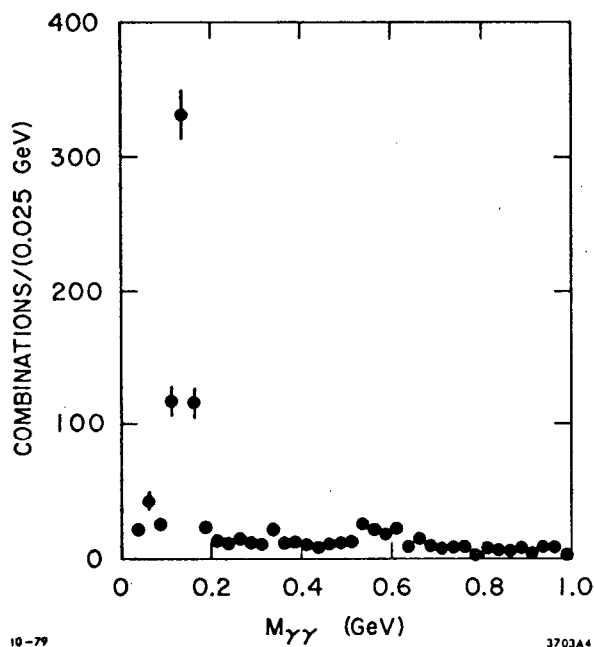pi^0$ cross section is consistent within errors with half the charged π cross section measured between $x = 0.3$ and 0.8.

From the measured π^0 distributions, predictions are made for the expected γ momentum distributions. In addition to the contribution from π^0 decays, there is an additional contribution from η decays.[7] Figure 8 shows the invariant mass distribution for $\gamma\gamma$ combinations with $x > 0.8$. In addition to the clear π^0 peak, one observes a signal in the region of the η. To determine the η population, least-squares fits to the $\gamma\gamma$ invariant mass distributions in different momentum bins are made. The functional form used in fitting the distributions consists of a Gaussian, fixed at the η mass with width as determined by Monte Carlo calculation, over a background whose shape is determined by the pseudo-photon combinations as described above. The ratio $R(p) = B(\psi \to \eta + X) \times B(\eta \to \gamma\gamma)/B(\psi \to \pi^0 + X)$ is measured as a function

Fig. 8. Invariant mass distribution for γγ combinations with the requirement that x > 0.8 for the γγ system.

of momentum. R(p) is found to be less than 0.10 for all momentum bins except for p > 1.2 GeV where R = 0.16 ± 0.06. (Possible systematic effects due to errors in the assumptions made about the shape of the background are not included in this error.) From the measured value of R as a function of momentum, the contribution to γ production from η's is estimated.

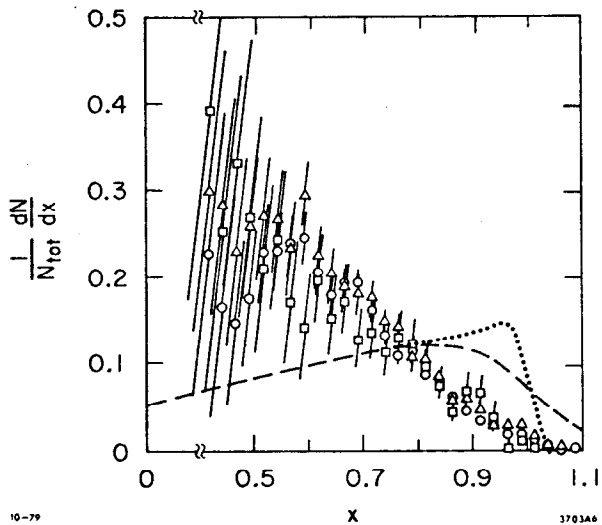The resulting predicted γ momentum distributions are shown in Fig. 6 along with the measured distributions. The error bars include a systematic error of ±22%. This error does not include correlated errors which affect the γ and π^o distributions similarly. The major contributions to this error are the uncertainty in the π^o detection efficiency and the background subtraction. Excess production of γ's over the prediction is observed for x > 0.5.

Figure 9 shows the direct γ momentum distributions calculated by subtracting the expected distributions from the measured distributions. The error bars include the statistical error and the systematic error in the difference between the measured and predicted distributions. The errors become small at large x because the π^o contribution is small. Since the error bars at the lower values of x are dominated by the systematic errors, the extent of the error bars should be considered as defining an envelope within which the actual distribution lies. For x < 0.4, the errors become too large to provide meaningful information, and only for x > 0.5 can a

Fig. 9. Direct γ momentum distributions. The symbol convention is identical to that used in Fig. 6. The solid curve is the leading-order QCD prediction convoluted with the energy resolution for LA γ's. The dashed curve is the same theoretical distribution convoluted with the energy resolution for converted γ's.

clear excess be demonstrated. In addition to the displayed error bars, there is a $\pm(17\text{-}20)\%$ systematic error (depending on the method of analysis) due to uncertainties in the γ detection efficiency, the number of produced ψ events, the trigger efficiency, and the angular distribution of the direct γ's as discussed below. The expected theoretical distribution (convoluted with the energy resolution for γ's detected in the LA and converted γ's) is also shown in Fig. 9. While the effect observed in the data is seen to be of approximately the same magnitude as one expects from theory, the shape of the observed distribution is softer. This is not unexpected in light of the earlier discussion on second-order corrections.

Figure 10 shows the distribution of observed photons (using method 3 only) with $x > 0.6$ as a function of $|\cos\theta|$, where θ is the polar angle of the γ with respect to the beam direction. The angular distribution has been fit to the form $1 + \alpha_\gamma \cos^2\theta$ and gives $\alpha_\gamma = 0.14 \pm 0.12$. Approximately 25% of these events are background from π^o or η decays. Analysis of the angular distribution of photons from observed π^o decays shows this background to be consistent with an isotropic distribution. Correcting for this background gives $\alpha_\gamma = 0.18 \pm 0.18$ for the direct γ contribution. An overall correction of 3% is made to the data (which has been included in Fig. 9) to correct for
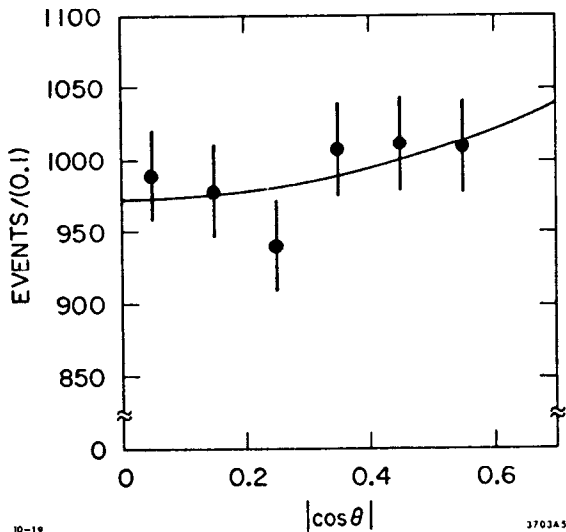
Fig. 10. Angular distribution of observed photons with x > .0.6 as a function of $|\cos\theta|$. Curve represents the best fit to the form $1 + \alpha_\gamma \cos^2\theta$.

the deviation of the observed angular distribution from isotropy.

Integrating the direct γ momentum distribution from x = 0.6 to 1.0, the Mark II obtains an inclusive rate for direct photon production of $(4.4 \pm 1.0)\%$ from method 1, $(3.9 \pm 1.2)\%$ from method 2, and $(4.1 \pm 0.8)\%$ from method 3. These integrated cross sections include a correction (-6% for methods 1 and 3) for feeddown from lower x due to the resolution of the LA. The best estimate of the branching fraction from these three measurements is $(4.1 \pm 0.8)\%$. This is to be compared with the theoretical expectation of 5% integrated over the same region in x. The angular distribution of the photons is uniquely determined from the calculation. α_γ is a function of x and reaches the value 1 at x = 1. The mean value of α_γ convoluted with the momentum distribution from x = 0.6 to 1.0 is expected to be approximately 0.3 which is in agreement with the data.

IV. Charmed Baryon Production

The Mark II collaboration has analyzed a sample of high-energy events for evidence of charmed baryon production and observes a signal in the $pK^-\pi^+$ final state at a mass of 2.285 GeV. The data sample used in the analysis represents an integrated luminosity of 5150 nb^{-1} obtained during a run at the fixed center-of-mass energy (E_{cm}) 5.2 GeV and 4000 nb^{-1} obtained during a scan of the region from 4.5 to 6.0 GeV. Particle identification is accomplished by the time-of-flight (TOF) system. The measured resolution

for hadron tracks of $\sigma = 0.30$ ns allows a $1-\sigma$ separation for $K-\pi$ at 1.35 GeV and for $K-p$ at 2.0 GeV momentum.

Figure 11(a) shows the invariant mass distribution for the $pK^-\pi^+$ and charge conjugate $\bar{p}K^+\pi^-$ combinations with the requirement that the mass recoiling against the $pK\pi$ system be greater than 2.2 GeV. A significant enhancement is observed at 2.285 GeV in these channels which have the quantum numbers of the Cabibbo-favored weak decay of the Λ_c. Figure 11(b) shows the complementary mass distribution for those $pK\pi$ combinations with recoil mass less than 2.2 GeV. No enhancement is observed in Fig. 11(b), indicating that the observed signal is associated with an equal or larger recoil mass. (Approximately one-fourth of the events are observed to have an equal mass recoil.) Figure 11(c) shows the invariant mass distribution for
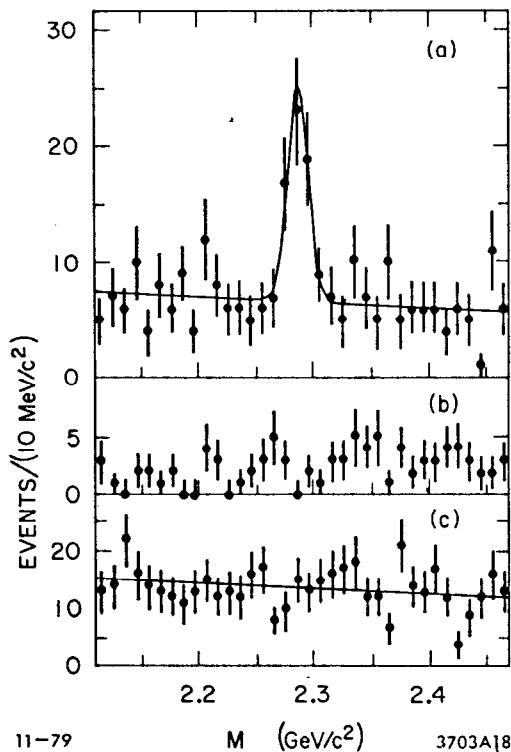

Fig. 11. The combined $pK^-\pi^+$ and $\bar{p}K^+\pi^-$ mass distribution for events with (a) recoil mass greater than 2.2 GeV, and (b) recoil mass less than 2.2 GeV. (c) The combined $pK^+\pi^-$ and $pK^-\pi^-$ (and charge conjugate states) mass distribution for events with recoil mass greater than 2.2 GeV. Curves are discussed in text.

the channels $pK^+\pi^-$ and $pK^-\pi^-$ and their charge conjugates with the same recoil mass cuts as used in Fig. 11(a). These channels have quantum numbers inconsistent with a Λ_c decay and do not exhibit any structure. The curve in Fig. 11(a) shows that the data are well fit to a Gaussian plus a background shape determined from a fit to Fig. 11(c). The signal consists of 39 ± 8 events above a background of 20 events.

The fit to Fig. 11(a) yields a mass of 2.286 ± 0.007 GeV and an rms width of 0.010 GeV. The quoted error includes a systematic component of 0.006 GeV due to uncertainties in the magnetic field and the geometrical reconstruction. These sources of error have been checked by measurement of the K^O and D^O masses in the data sample. A shift in the mass of the observed $pK\pi$ signal of 0.003 GeV, for example, would require a change in the magnetic field which would displace these masses from their present agreement with nominal values by one standard deviation (0.001 GeV for M_{K^O} and 0.0025 GeV for M_{D^O}). The mass has also been determined by making a beam-energy constraint to events in which the total measured energy of the $pK\pi$ system is within 0.03 GeV of the beam energy. The mass determined in this manner is 2.284 ± 0.008 GeV. This mass determination is subject to different systematic errors than the invariant mass and is combined with that mass value to give the best estimate of 2.285 ± 0.006 GeV for the mass of the observed state. As expected for the weak decay of a charmed baryon, the measured width agrees with the calculated detector resolution.

In the cross section analysis, only the sample of events observed in the 5450 nb^{-1} integrated luminosity within 0.05 GeV of 5.2 GeV E_{cm} is used. The detection efficiency has been calculated for the observed Λ_c momentum distribution to be 0.13 ± 0.025. The 26 ± 7 observed signal events correspond to

$$\left[\sigma(\Lambda_c) + \sigma(\bar{\Lambda}_c)\right] \times B(\Lambda_c \to pK^-\pi^+) = 0.037 \pm 0.012 \text{ nb} \quad .$$

In order to estimate the absolute branching fraction of the Λ_c into $pK\pi$, it is necessary to make a few assumptions regarding charmed baryon decays and inclusive proton production. The inclusive antiproton cross section has been measured between 3.52 and 7.40 GeV. Because of substantial beam-gas contamination in the proton events, only antiprotons are used for these measurements. Two or more observed tracks are required in the event and

valid identification of antiprotons by TOF is required. The efficiency

for detection of antiprotons is calculated by Monte Carlo and the overall

detection efficiency is approximately 60% over the entire energy range from

3.5 to 7.4 GeV.

The resulting inclusive proton production cross section as a function

of energy is presented in Fig. 12 as the ratio of the inclusive cross

section to the μ-pair cross section, $R(p + \bar{p}) = 2\sigma(\bar{p})/\sigma_{\mu\mu}$. Error bars

represent the statistical errors only. The estimated ±17% systematic

error is dominated by the model dependence of the Monte Carlo calculations,

and is expected to vary slowly over the energy region. Within the quoted

errors, this measurement is consistent with the results of previous experi-

ments.[8] One sees a step in $R(p + \bar{p})$ which starts below 5.0 GeV and which is

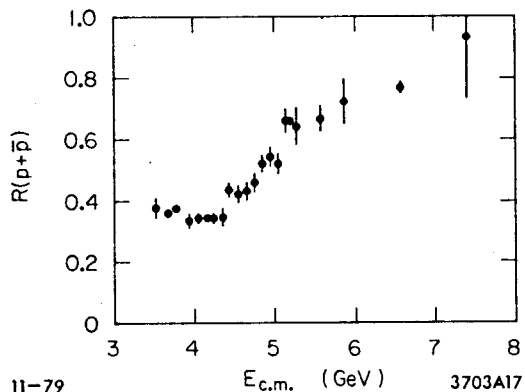assumed to be associated with the onset of charmed baryon production.

Fig. 12. $R(p + \bar{p})$ as a function of E_{cm}.

The measurement of $R(p + \bar{p})$ and the measured value of $\sigma \cdot B$ for the $pK\pi$ signal at 5.2 GeV can be used to estimate the absolute branching ratio for the $pK\pi$ decay mode. The following assumptions are made: (i) The observed step in $R(p + \bar{p})$ is due entirely to charmed baryon pair production. (ii) All charmed baryons cascade down to the Λ_c state. (iii) The probability for a charmed baryon to give a proton (as opposed to a neutron) as a final

product is 0.6 ± 0.1. This value is slightly model dependent and is estimated

from a measurement of inclusive proton and Λ cross sections and a simple

isospin statistical model. Using the relationship

$$\left[\sigma(\Lambda_c) + \sigma(\bar{\Lambda}_c) \right] = \frac{\Delta R(p + \bar{p})}{0.6} \sigma_{\mu\mu}$$

and the measured step in $R(p + \bar{p}) = 0.31 \pm 0.06$, the Mark II finds an inclusive

cross section $\sigma(\Lambda_c) + \sigma(\bar{\Lambda}_c) = 1.7 \pm 0.4$ nb at 5.2 GeV. With these assumptions,

the branching ratio is then estimated to be $B(\Lambda_c \to pK^- \pi^+) = (2.2 \pm 1.0)\%$.

V. Crystal Ball Results

The Crystal Ball[9] is a large solid angle detector with good efficiency

and resolution for photon detection at all energies. A schematic of the

Crystal Ball detector is shown in Fig. 13. The detector consists of two

DETECTOR COMPONENTS OF THE
CRYSTAL BALL-SLAC 1978
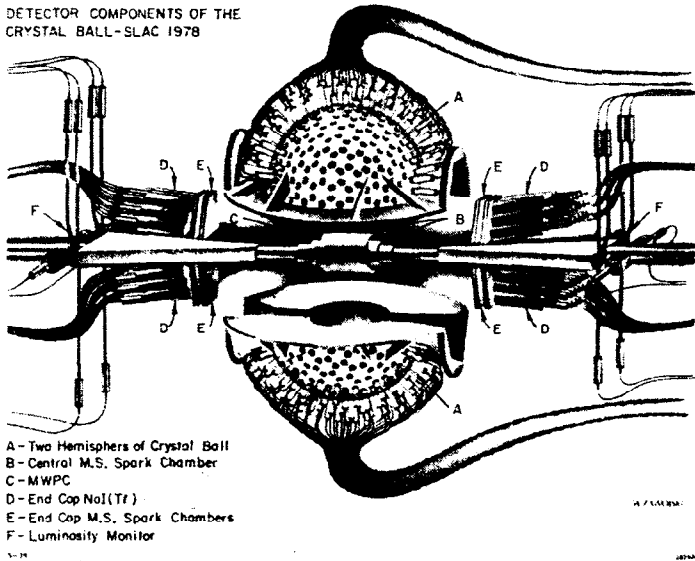
A - Two Hemispheres of Crystal Ball
B - Central M.S. Spark Chamber
C - MWPC
D - End Cap NaI(Tℓ)
E - End Cap M.S. Spark Chambers
F - Luminosity Monitor

Fig. 13. Schematic of the components of the
         Crystal Ball detector.

hemispheres, each containing 336 NaI(Tℓ) crystals 16-radiation lengths thick. This central part of the detector covers 94% of 4π sr. In addition, the detector has systems of magnetostrictive spark chambers and multiwire proportional chambers inside the ball. The endcap regions are

covered by additional magnetostrictive spark chambers and NaI(Tℓ) crystals

which increase the solid angle coverage of the detector to 98% of 4π sr.

The energy resolution was measured by using a prototype detector and is

approximately $\Delta E/E$ (FWHM) $= 0.028 \ E^{-\frac{1}{4}}$ (E in GeV). The resolution obtained

so far during experimental running is approximately a factor of two worse.
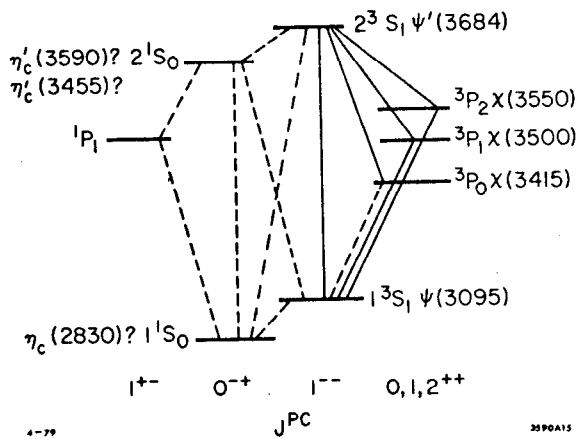
Fig. 14. The lowest lying charmonium levels and the observed states generally associated with them. Solid lines are observed transitions and dashed lines are expected transitions which are weak or unobserved.

Figure 14 shows the lowest lying charmonium levels and the observed states corresponding to these levels. The solid lines represent observed transitions, and the dashed lines represent expected transitions which are weak or unobserved. The ψ and ψ' are unambiguously identified as the vector meson ($^3S_1$) states. The χ states are generally associated with the ^3P levels. The major problem in the confrontation between theory and experiment is the identification of the pseudoscalar states associated with the ψ and the ψ'. Candidates for these states have been published in the literature,[10] but later experiments with greater sensitivity have not observed them.[11] Thus, it is still necessary to find evidence for the pseudoscalar states required by the theory. Preliminary results are presented here for a radiative transition from the ψ' to a state just below the ψ.

Figure 15 shows the inclusive γ spectrum from the ψ' as a function of γ energy. This data comes from a sample of 800,000 ψ' events. In order to reduce backgrounds in the data sample, γ's near the endcap region are not used in the analysis ($|\cos\theta| < 0.85$, where θ is the angle of the γ with respect to the beam axis). In addition, a minimum opening angle cut between charged particles and γ's is imposed ($\cos\theta_{\gamma X} < 0.85$). Finally, pairs of γ's with invariant mass consistent with the π^0 mass are eliminated from the data. Figure 15 clearly shows the three monochromatic lines due to the radiative transitions from the ψ' to the three χ states, and the Doppler-broadened lines due to transitions from the upper two χ states to the ψ. A fifth
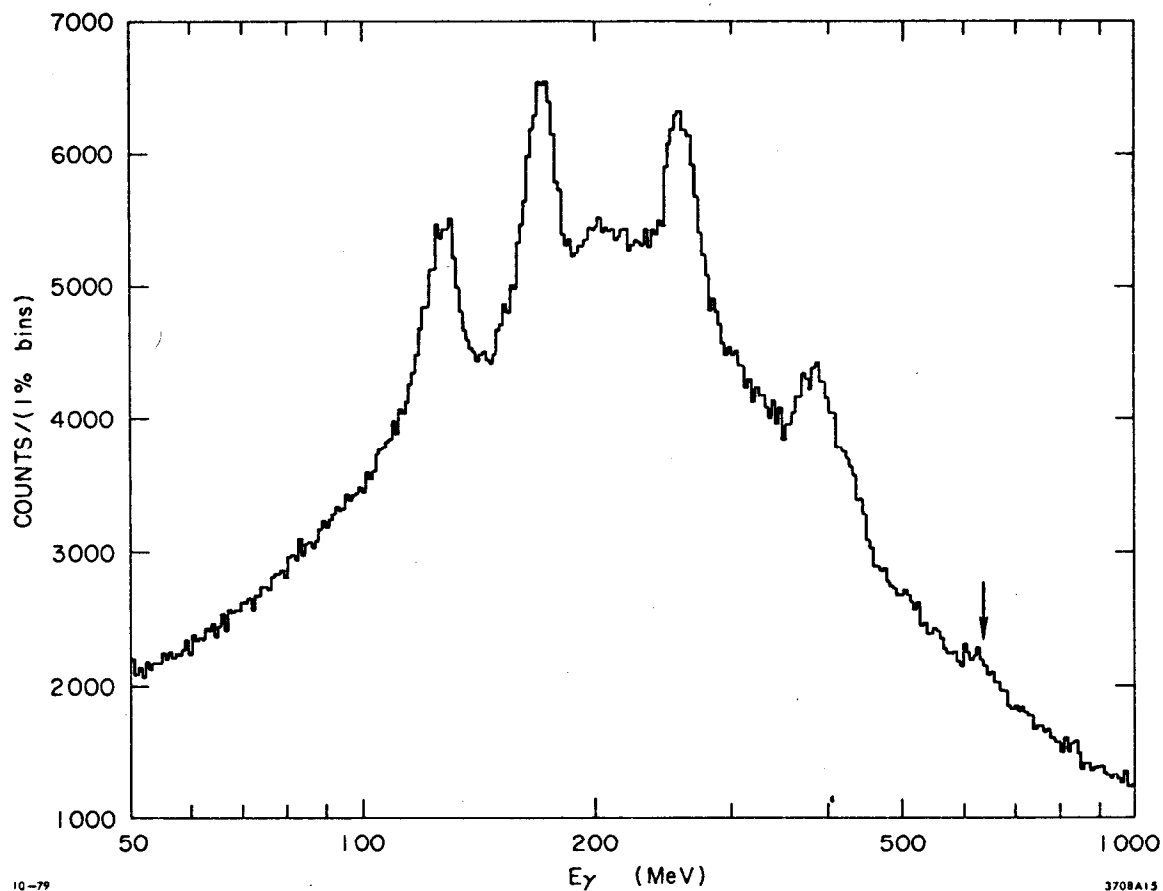
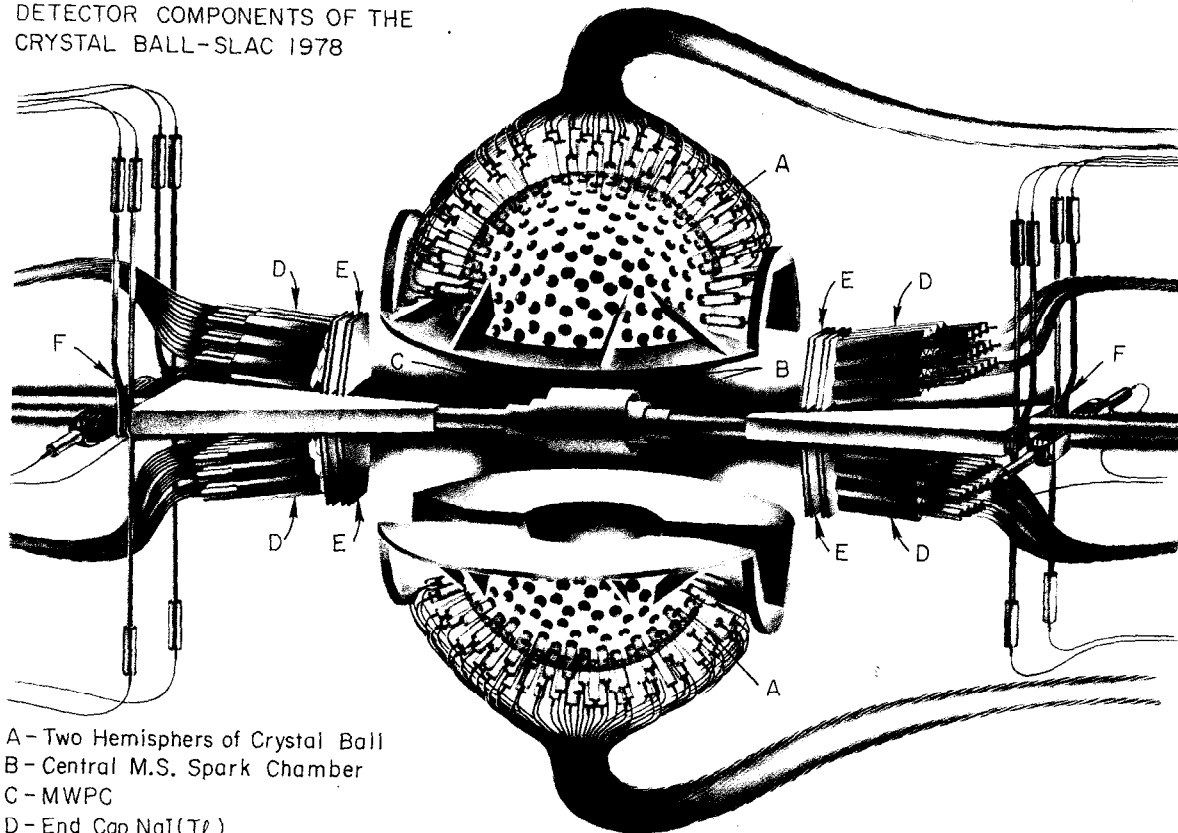Fig. 15. Inclusive γ distribution from the ψ' as a function of γ energy.

peak is seen near 640 MeV. The state has a mass of 2.98 ± 0.02 GeV. The width is consistent with the experimental resolution (60 MeV FWHM). The branching ratio is estimated to be (0.2-0.5)%. All measured parameters of this state are consistent with theoretical expectations for the η_c.

References

1. G. Abrams, M. Alam, C. Blocker, A. Boyarski, M. Breidenbach, D. Burke,
   W. Carithers, W. Chinowsky, M. Coles, S. Cooper, W. Dieterle, J. Dillon,
   J. Dorenbosch, J. Dorfan, M. Eaton, G. Feldman, M. Franklin, G. Gidal,
   G. Goldhaber, G. Hanson, K. Hayes, T. Himel, D. Hitlin, R. Hollebeek,
   W. Innes, J. Jaros, P. Jenni, D. Johnson, J. Kadyk, A. Lankford,
   R. Larsen, V. Lüth, R. Millikan, M. Nelson, C. Pang, J. Patrick,
   M. Perl, B. Richter, A. Roussarie, D. Scharre, R. Schindler,
   R. Schwitters, J. Siegrist, J. Strait, H. Taureg, M. Tonutti,
   G. Trilling, E. Vella, R. Vidal, I. Videau, J. Weiss, and H. Zaccone.

2. G. S. Abrams et al., Phys. Rev. Lett. 43, 477 (1979); G. S. Abrams et al.,
   Phys. Rev. Lett. 43, 481 (1979).

3. T. Appelquist et al., Phys. Rev. Lett. 34, 365 (1975); M. Chanowitz,
   Phys. Rev. D12, 918 (1975); L. Okun and M. Voloshin, ITEP-95-1976
   (unpublished); S. J. Brodsky et al., Phys. Lett. 73B, 203 (1978);
   K. Koller and T. Walsh, Nucl. Phys. B140, 449 (1978).

4. This calculation of α_s is based on the ratio of the hadronic and
   leptonic widths of the ψ [see T. Appelquist and H. D. Politzer, Phys.
   Rev. Lett. 34, 43 (1975)]. The predicted direct γ contribution is
   included in the total width of the ψ used in the calculation.

5. R. Barbieri et al., Nucl. Phys. B154, 535 (1979).

6. R. L. Ford and W. R. Nelson, SLAC Report No. 210, 1978 (unpublished).

7. The contribution from radiative decays of other secondary hadrons has
   been estimated to be small compared to the η contribution and negligible
   compared to the overall uncertainty in the π^o contribution.

8. R. Brandelik et al., Nucl. Phys. B148, 189 (1979); M. Piccolo et al.,
   Phys. Rev. Lett. 39, 1503 (1977).

9. The members of the collaboration are D. Aschman, E. D. Bloom, F. Bulos,
    T. Burnett, M. Cavalli-Sforza, R. Chestnut, D. Coyne, J. Gaiser,
    G. Godfrey, R. Hofstadter, C. Kiesling, I. Kirkbride, H. Kolanoski,
    W. Kollmann, A. Liberman, J. O'Reilly, M. Oreglia, R. Partridge, C. Peck,
    F. Porter, M. Richardson, H. Sadrozinski, K. Strauch, J. Tompkins, and
    K. Wacker.

10. A state at 3590 MeV was observed in the decay $\psi' \to \gamma\gamma\psi$ [W. Bartel et al.,
    Phys. Lett. 79B, 492 (1978)]. A state at 3455 MeV was observed in the
    same reaction [J. S. Whitaker et al., Phys. Rev. Lett. 37, 1596 (1976)].
    A state at 2830 MeV was observed in the decay $\psi \to \gamma\gamma\gamma$ [W. Braunschweig
    et al., Phys. Lett. 67B, 243 (1977)].

11. E. D. Bloom, SLAC-PUB-2425, presented at the 1979 International Symposium
    on Lepton and Photon Interactions at High Energy, Batavia, Illinois,
    August 23-29, 1979; G. S. Abrams et al., SLAC-PUB-2350, presented at
    the International Conference on High Energy Physics, Geneva, Switzerland,
    June 27 - July 4, 1979.

DETECTOR COMPONENTS OF THE
CRYSTAL BALL—SLAC 1978

A — Two Hemisphers of Crystal Ball
B — Central M.S. Spark Chamber
C — MWPC
D — End Cap NaI(Tℓ)
E — End Cap M.S. Spark Chambers
F — Luminosity Monitor

5—79

W. ZAWOJSKI

362641